Supplemental Materials

Molecular Biology of the Cell

Tang et al.

Supplemental Material

SM Model and Methods

1. Model Description

Equation of Motion. Actin filaments are helical polymer chains composed of actin monomers. To capture the mechanical properties of actin filaments, we use a coarse-grained spring-bead model to represent the actin filament, generalizing an earlier 2D model (Laporte *et al.*, 2012). In our model, a chain of beads that are connected by springs are free to move in 3D space, subject to mechanical forces (spring, bending, thermal) that maintain its shape and to additional forces from other proteins. We use Langevin dynamics (Pasquali *et al.*, 2001; Nédélec and Foethke, 2007) to update the bead positions $\mathbf{r}_i$ of the i^{th} bead in simulation time dt:

$$\mathbf{F}_i^{spring} + \mathbf{F}_i^{bend} + \mathbf{F}_i^{thermal} + \mathbf{F}_i^{crslnk} + \mathbf{F}_i^{myo} = \zeta_b \frac{dr_i}{dt}, i = 1,2,..N \qquad (1)$$

The different forces are described below. Spring, bending and thermal forces are intrinsic to the actin filament properties, while cross-linking and myosin walking forces are due to the effects of other proteins. ζ_b is an effective drag coefficient of a filament segment in cytoplasm. Each segment is 0.1 µm, representing about 37 subunits.

Spring force. The spring force exerted on the i^{th} bead from the neighboring two springs is calculated as:

$$\mathbf{F}_i^{spring} = -\frac{\partial E^{spring}}{\partial r_i} = -\frac{k}{2}\sum_{j=1}^{N-1}\frac{\partial\left(|\mathbf{r}_{j+1}-\mathbf{r}_j|-l_0\right)^2}{\partial \mathbf{r}_i} \qquad (2)$$

where E^{spring} is the total spring energy and l_0 is the equilibrium length (0.1 µm). The stiffness k of a 0.1-µm-long actin filament is 437 pN/nm, ten times bigger than that of a 1-µm-long actin filament since $k = ES/l_0$, where E is the Young's modulus and S is the cross-sectional area of an actin filament (Kojima *et al.*, 1994). We use a much smaller k = 100 pN/µm in the simulation that is enough to suppress extensile stretching while at the same time allowing us to use a larger dt so that the simulations are more efficient.

Bending force. The bending force is calculated by measuring the local deformation of neighboring beads.

$$\mathbf{F}_i^{bend} = -\frac{\partial E^{bend}}{\partial \mathbf{r}_i} = -\frac{\kappa}{l_0}\sum_{j=1}^{N-1}\frac{\partial(\mathbf{t}_j \cdot \mathbf{t}_{j-1})}{\partial \mathbf{r}_i} \qquad (3)$$

where E^{bend} is the elastic bending energy, $\mathbf{t}_i \equiv \frac{\mathbf{r}_{j+1}-\mathbf{r}_j}{|\mathbf{r}_{j+1}-\mathbf{r}_j|}$ is the local unit tangent vector, κ is the flexural rigidity, $\kappa = k_B T l_p$, where k_B is Boltzmann's constant, T is temperature (we use 300 K (Laporte *et al.*, 2012)) and l_p is the persistence length of the filament (Gittes *et al.*, 1993). We tested that the simulated filaments do have the same persistence length as in Eq. (3) in the next section.

Thermal force. The thermal force represents random fluctuating forces acting on the filament and satisfy:

$$\langle \mathbf{F}_i^{thermal} \cdot \mathbf{F}_i^{thermal^T} \rangle_{\alpha,\beta} = \frac{2k_B T \zeta_b}{\Delta t}\hat{I}_{\alpha,\beta} \qquad (4)$$

where $\hat{I}_{\alpha,\beta}$ is the second-order unit tensor, and Δt is the simulation time step (Pasquali *et al.*, 2001; Nédélec and Foethke, 2007).

Polymerization. We assume a constant total number of formin dimers at the cell tips (72 at each end). These formins are distributed into $N_{cluster}$ clusters. Each cluster contains $72/N_{cluster}$ formin dimers. Changing $N_{cluster}$ we are able to evaluate the clustering effect of the formins. The clusters are chosen to be randomly distributed on the cell tip surfaces. Formins within the same cortical site are distributed randomly over a small area around the center of the site. Polymerization of filaments is simulated as elongation of the segments attached to the formin nucleation sites. We use a polymerization rate v_p = 0.3 µm/s (Lo Presti *et al.*, 2012). If the elongating segment reaches twice the size of spring equilibrium length l_0, a new bead is added to the middle of the segment.

Cross-linking. Cross-linking is simulated as attraction between beads that come close to one another. The cross-linking force, $\mathbf{F}_i^{crslnk}$, when bead i is within r_{crslnk} of bead j (belonging to the same or different filament) is defined as:

$$\mathbf{F}_i^{crslnk} = -\frac{k_{crslnk}}{2}\sum_j \frac{\partial\left(|\mathbf{r}_i-\mathbf{r}_j|-r_0\right)^2}{\partial \mathbf{r}_i}, \qquad \text{for } \left|\mathbf{r}_i - \mathbf{r}_j\right| \le r_{crslnk}, \qquad (5)$$

where the interaction range r_{crslnk} and interaction spring constant k_{crslnk} are varied in the simulations. r_{crslnk} and k_{crslnk} characterize the binding/unbinding kinetics of the cross-linkers and their concentration. We use $r_0 = 0.03$ µm as the equilibrium distance between the two cross-linked filament beads, which represents an effective distance between two actin segments cross-linked by cross-linkers such as α–actinin or fimbrin (Klein *et al.*, 2004; Sjoblom *et al.*, 2008).

Filament turnover. Here we employ a simplified mechanism for filament turnover: we remove whole filaments with a rate that gives an average filament lifetime 15s (Vavylonis *et al.*, 2008). In the simulation, filaments are tested for removal every 0.001 s. Other than cofilin, For3p dissociation from cell tips may also contribute to actin filament turnover (Wang and Vavylonis, 2008).

Fission yeast shape. Fission yeast during G2 phase has a rod-like shape with a diameter of 3 to 4 µm and a length of 7 to 12 µm. In our simulations, we use a cylinder capped by two hemispheres (tips), with a diameter of 3.6 µm and length of 9 µm (end to end) to represent the shape. We simulate the boundary as a hard wall by a large repelling force applied to filament beads crossing the cell boundary.

Excluded volume. Excluded volume by the larger organelles such as the vacuoles and the nucleus is simulated by immobile spheres that prevent actin filaments from going through them. We used 2.4 µm as the diameter of the nucleus at the center. The vacuoles are simulated as spheres randomly distributed in the remaining volume. The volume fraction occupied by the spheres (excluding nucleus) is 17.14%, consistent with the 10%-20% measurements in (Milo, 2013). We note that the vacuole volume can drastically change in different medium or under osmotic pressure (Bone *et al.*, 1998). The diameter of the spheres is 0.8 µm, based on electron tomography (Hoog *et al.*, 2007), giving a total number of 40. This is bigger than 0.4 µm reported in (Bone *et al.*, 1998; Mulvihill *et al.*, 2001) and the number of spheres 40 is smaller than the number of vacuoles counted in (Bone *et al.*, 1998; Mulvihill *et al.*, 2001).

Myosin pulling. We assume 0.5 pN force per myosin V (Mehta *et al.*, 1999) and 5 s association time. We vary the density of motors per µm, ρ_{myo}, along the filament to observe the effects of myosin V pulling under different myosin V concentrations. We simulate the effects of attached myosin V on the i^{th} bead of a filament as a transient tangential force towards the barbed end:

$$\mathbf{F}_i^{myo} = -F_{myo}\,\mathbf{t}_{i-1} \qquad (6)$$

Distribution of Cortical Sites and For3p Dimers within Cortical Sites. The cortical cluster sites are randomly distributed on the semi-spherical cell tips. Formin For3p dimers are found distributed in landmark protein clusters on the tips (Martin and Chang, 2006). In our simulations, formin dimers within the same cortical site are distributed randomly within a small area. For 6 formin dimers per cluster, the diameter of the cortical site is 0.1 μm.

2. Validation of Single Actin Filament Model

Before applying interactions with other proteins and boundary conditions, we tested the mechanical properties of individual filaments to reproduce known expressions for the tangent correlation function, relaxation dynamics and elastic energy.

Tangent Correlation. The shape of an actin filament of length L can be represented by a parametric 3D curve $\boldsymbol{r}(x,t)$, where x is the contour length along the filament ($0 \le x \le L$) and t is the time. In thermal equilibrium we have:

$$\langle \mathbf{t}(x)\mathbf{t}(x+\Delta x)\rangle = e^{-\Delta x(D-1)/2l_p} \qquad (7)$$

where $\mathbf{t}(x) = d\mathbf{r}/dx$ is the unit tangent vector along its contour, $D = 3$ is the dimension of free space, and l_p is the persistence length. The persistence length is given by $l_p = k_B T/\kappa$, where T is temperature and κ is the flexural rigidity of the filament,. Actin filaments in vitro have a persistence length of about 10 µm (Gittes *et al.*, 1993), which is what we used throughout the simulations.

Figure S1 shows our simulations of single filaments of constant length maintain the persistence length of filaments initialized with equilibrium configurations. Figure S1A shows that filaments can be initialized with a defined persistence length satisfying Eq. (7). Figure S1B shows that use of Langevin dynamics to evolve such filaments over times longer than the longest relaxation time τ maintains the persistence length and the shape of the tangent correlation function of Eq. (7).

Relaxation Dynamics. To test that our simulations reproduce the known dynamics of single worm-like chains, we expanded the filament space curve using an orthonormal set $\{Q_n(x)\}$:

$$\mathbf{r}(x,t) = \sum_n \mathbf{q}_n(t) Q_n(x), \quad n = 1,2,\ldots \tag{8}$$

where the orthonormal set is (Fujime and Maruyama, 1973):

$$Q_1(x) = \left(\frac{12}{L^3}\right)^{\frac{1}{2}} \left(\frac{L}{2} - x\right)$$
$$Q_n(x) = L^{-\frac{1}{2}} \left[(\cos\alpha_n x + \cosh\alpha_n x) - \frac{\cos\alpha_n L - \cosh\alpha_n L}{\sin\alpha_n L - \sinh\alpha_n L}(\sin\alpha_n x + \sinh\alpha_n x)\right], \ n \geq 2 \tag{9}$$

where L is filament length and the coefficient $\alpha_n = \left(n - \frac{1}{2}\right)\frac{\pi}{L}$. Thus vector $\mathbf{q}_n(t)$ is a complete representation of the filament shape.

For a given time difference τ, we calculate the correlation coefficient $R_{q_n}(\tau)$ (Figure S2A):

$$R_{q_n}(\tau) = \frac{\langle \mathbf{q}_n(0)\mathbf{q}_n(\tau)\rangle}{\langle \mathbf{q}_n(0)\mathbf{q}_n(0)\rangle} = \frac{\frac{1}{T-\tau}\int_0^{T-\tau} dt[\mathbf{q}_n(t) - \bar{\mathbf{q}}_n][\mathbf{q}_n(t+\tau) - \bar{\mathbf{q}}_n]}{\frac{1}{T}\int_0^{T} dt[\mathbf{q}_n(t) - \bar{\mathbf{q}}_n]^2} \tag{10}$$

where $\bar{\mathbf{q}}_n$ is the time average of $\mathbf{q}_n(t)$. From the fluctuation-dissipation theorem (Fujime and Maruyama, 1973), we also have:

$$\langle \mathbf{q}_n(0)\mathbf{q}_n(\tau)\rangle = \langle \mathbf{q}_n(0)\mathbf{q}_n(0)\rangle e^{-\tau/\tau_n} \tag{11}$$

We fit $R_{q_n}(\tau)$ to the exponential decay $e^{-\tau/\tau_n}$ to get the simulated relaxation time τ_n for mode *n* (Figure S2B). We compare this value to the calculated theoretical value for τ_n (Fujime and Maruyama, 1973) (Figure S2B):

$$\tau_n = \frac{\zeta/l_0}{k_B T l_p} \frac{L^4}{(n-1/2)^4 \pi^4} \tag{12}$$

where $\zeta/l_0$is the drag coefficient per segment length (i.e. per filament bead). In our simulations the drag coefficient per bead is the drag coefficient of a rod of segment l_0 for movement perpendicular to the rod axis, as in (Laporte *et al.*, 2012):

$$\zeta = 4\pi\eta l_0/[0.84 + \ln(\frac{l_0}{2a})] \tag{13}$$

where η is the viscosity. Figure S2B shows good accordance between our simulated data and calculation from theory. We also varied the temperature *T*, filament segment length l_0, and persistence length l_p to find that the calculated relaxation times are all in agreement with theory (Figure S2C, D, E).

Equipartition of Energy. The elastic bending energy of the filament polymer chain is given by (Fujime and Maruyama, 1973):

$$\langle V\rangle = \langle \frac{1}{2}\int_0^L \left\{\kappa\left(\frac{\partial^2 \boldsymbol{r}}{\partial x^2}\right)^2\right\} dx\rangle = \frac{1}{2}\sum_n \lambda_n \langle \boldsymbol{q}_n(0)\boldsymbol{q}_n(0)\rangle \tag{14}$$

By equipartition theory, one has (Fujime and Maruyama, 1973):

$$\langle \boldsymbol{q}_n(0)\boldsymbol{q}_n(0)\rangle = \langle {\boldsymbol{q}_n}^2\rangle = 3k_B T/\lambda_n \tag{15}$$

where

$$\lambda_n = \kappa[\frac{(n-1/2)\pi}{L}]^4, \text{ with } \kappa = k_B T l_p \tag{16}$$

Figure S2F shows a comparison of the energy per mode from theory from Eqs. (15) and (16) with the energy in our simulations calculated using Eq. (14).

3. Quantification of Simulation Results.

Here we describe how we measured the number of filaments in the largest linked cable, the percent of bundled filaments and cable number in the simulations. If more than 15 beads (1.5 μm) of two filaments are cross-linked (gap $\leq r_{crslnk}$), these two filaments are defined to form a "pair". A "bundle" is defined as a set of filaments that have pairs within the set; a bundle also contains all pairs of filaments in the set and cannot be reduced to a smaller set of two or more bundles. The number of filaments in the largest linked cable (Figure 7B, Figure S3A, Figure S4A) equals the number of the filaments of the bundle with the most filaments. The bundled percentage (Figure 3C, Figure 4B, Figure 7C) is the sum of all the filaments in different bundles divided by the total number of filaments (144). The cable number (Figure 4C, Figure 7D, Figure S3B, Figure S4B) is the total number of bundles.

4. Effect of cross-linker-dependent filament turnover rate

We performed simulations to study the effect of decreased actin filament disassembly with increased bundling, to explore the effect of reduction of filament disassembly due to cross-linking (Schmoller *et al.*, 2011). We implemented a dynamic turnover rate: average filament removal rates are $1/10\text{s}^{-1}$, $1/12.5\text{s}^{-1}$, $1/15\text{s}^{-1}$, $1/17.5\text{s}^{-1}$, $1/20\text{s}^{-1}$ for total bundled filament length (l_b in μm) of $l_b < 1$, $1 < l_b < 3$, $3 < l_b < 5$, $5 < l_b < 8$, $l_b > 8$. The results are shown in Figure S8 (in all other simulations in this paper we have a fixed turnover rate $1/15\ \text{s}^{-1}$). We found bundled percentages are similar for both fixed and dynamic turnover rates (Figure S8A). The average filament length in the dynamic turnover case is however shorter in the low bundled phase (low k_{crslnk}) and longer in the high bundled phase (high k_{crslnk}) compared to the case with fixed turnover rate (Figure S8B and C). These results indicate that our conclusions with fixed turnover rate are robust even when the lifetime of actin filaments changes by a factor of two as a result of cross-linking.

References

Bone, N., Millar, J.B., Toda, T., and Armstrong, J. (1998). Regulated vacuole fusion and fission in Schizosaccharomyces pombe: an osmotic response dependent on MAP kinases. Curr Biol *8*, 135-144.

Fujime, S., and Maruyama, M. (1973). Spectrum of Light Quasielastically Scattered from Linear Macromolecules. Macromolecules *6*, 237-241.

Gittes, F., Mickey, B., Nettleton, J., and Howard, J. (1993). Flexural rigidity of microtubules and actin filaments measured from thermal fluctuations in shape. J. Cell Biol. *120*, 923-934.

Hoog, J.L., Schwartz, C., Noon, A.T., O'Toole, E.T., Mastronarde, D.N., McIntosh, J.R., and Antony, C. (2007). Organization of interphase microtubules in fission yeast analyzed by electron tomography. Dev Cell *12*, 349-361.

Klein, M.G., Shi, W., Ramagopal, U., Tseng, Y., Wirtz, D., Kovar, D.R., Staiger, C.J., and Almo, S.C. (2004). Structure of the actin crosslinking core of fimbrin. Structure *12*, 999-1013.

Kojima, H., Ishijima, A., and Yanagida, T. (1994). Direct measurement of stiffness of single actin filaments with and without tropomyosin by in vitro nanomanipulation. Proc Natl Acad Sci U S A *91*, 12962-12966.

Laporte, D., Ojkic, N., Vavylonis, D., and Wu, J.Q. (2012). alpha-Actinin and fimbrin cooperate with myosin II to organize actomyosin bundles during contractile-ring assembly. Mol Biol Cell *23*, 3094-3110.

Lo Presti, L., Chang, F., and Martin, S.G. (2012). Myosin Vs organize actin cables in fission yeast. Mol Biol Cell *23*, 4579-4591.

Martin, S.G., and Chang, F. (2006). Dynamics of the formin for3p in actin cable assembly. Curr. Biol. *16*, 1161-1170.

Mehta, A.D., Rock, R.S., Rief, M., Spudich, J.A., Mooseker, M.S., and Cheney, R.E. (1999). Myosin-V is a processive actin-based motor. Nature *400*, 590-593.

Milo, R. (2013). What is the total number of protein molecules per cell volume? A call to rethink some published values. Bioessays *35*, 1050-1055.

Mulvihill, D.P., Pollard, P.J., Win, T.Z., and Hyams, J.S. (2001). Myosin V-mediated vacuole distribution and fusion in fission yeast. Curr Biol *11*, 1124-1127.

Nédélec, F., and Foethke, D. (2007). Collective Langevin dynamics of flexible cytoskeletal fibers. New Journal of Physics *9*, 427-451.

Pasquali, M., Shankar, V., and Morse, D.C. (2001). Viscoelasticity of dilute solutions of semiflexible polymers. Phys. Rev. E *64*, 020802.

Schmoller, K.M., Semmrich, C., and Bausch, A.R. (2011). Slow down of actin depolymerization by cross-linking molecules. J Struct Biol *173*, 350-357.

Sjoblom, B., Salmazo, A., and Djinovic-Carugo, K. (2008). Alpha-actinin structure and regulation. Cell Mol Life Sci *65*, 2688-2701.

Vavylonis, D., Wu, J.Q., Hao, S., O'Shaughnessy, B., and Pollard, T.D. (2008). Assembly mechanism of the contractile ring for cytokinesis by fission yeast. Science *319*, 97--100.

Wang, H., and Vavylonis, D. (2008). Model of For3p-mediated actin cable assembly in fission yeast. PLoS ONE *3*, e4078.

SM Figures.

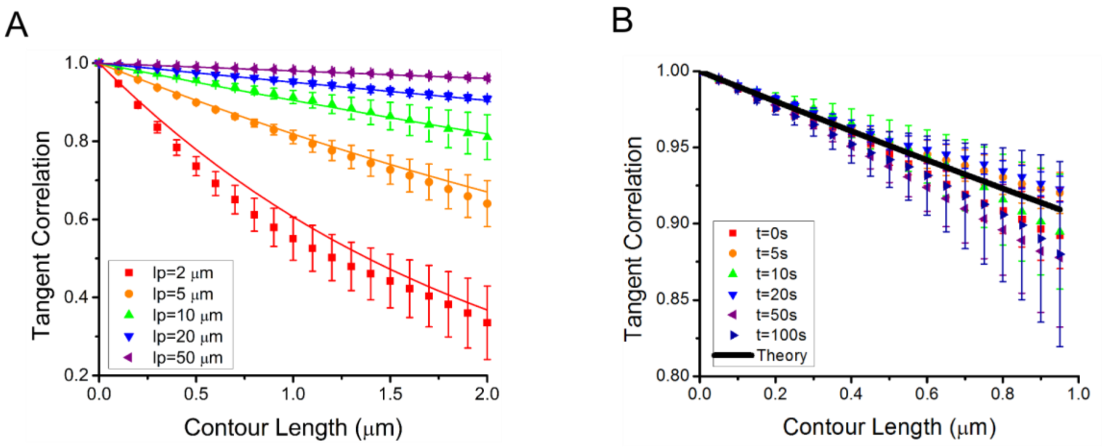

Figure S1. Validation of simulation methods using tangent correlation analysis of a single actin filament at initialization and during time-evolution. Theoretical calculation (solid lines) is given by $e^{-\Delta x/l_p}$. Simulated filaments are initialized in equilibrium (fully relaxed). All error bars are standard error (SEM) from five simulations. (A) Comparison of tangent correlation function of initialized filaments of length 10 μm with persistence lengths l_p 2-50 μm. (B) Evolution of tangent correlation in time for an isolated 2 μm actin filament with persistence length l_p = 10 μm initialized in equilibrium. The tangent correlation function remains unchanged from the equilibrium shape during simulations. We tested t = 0 – 100 s. The theoretical longest relaxation time is 4.5s.

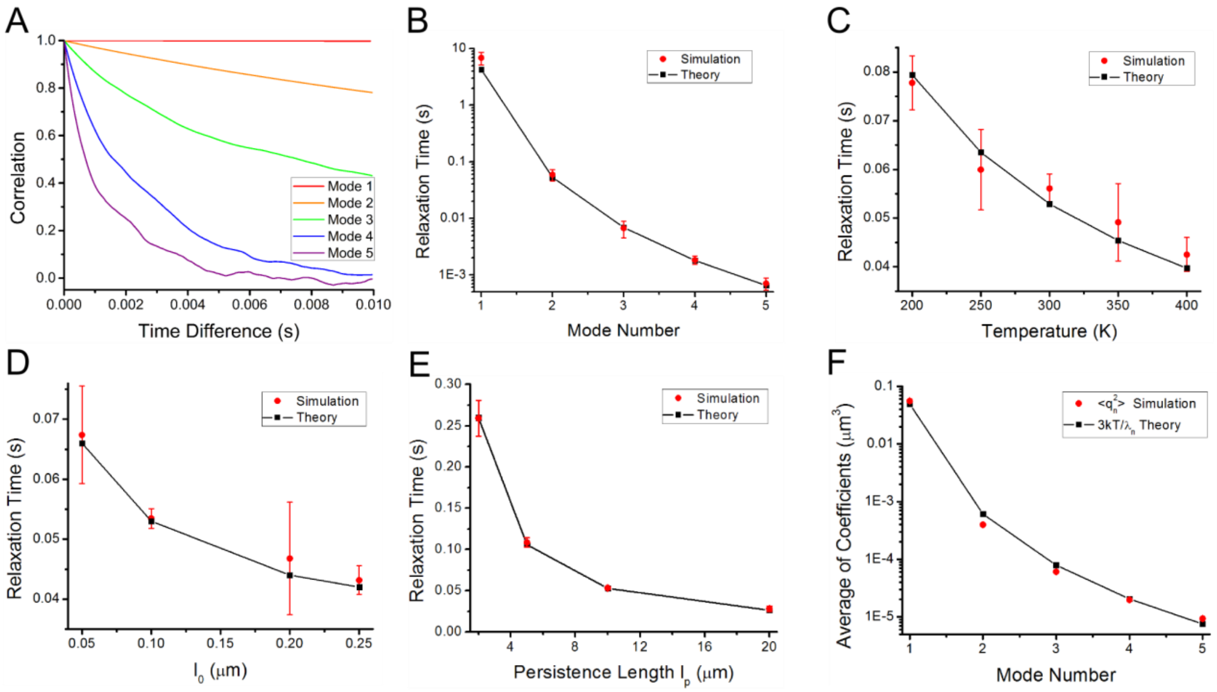

Figure S2. Validation of simulation methods using tests for relaxation dynamics and energy equipartition for a simulated individual actin filament of 2 µm with persistence length l_{p} = 10 µm, l_0 = 0.2 µm, at T = 300K unless varied. All error bars are SEM from 5 runs. (A) The time correlation of coefficients $\{\mathbf{q}_n(t)\}$ of expansion in space $\{Q_n(x)\}$ for modes n = 1-5. (B) Relaxation time calculation from exponential fits to simulation results in panel A compared to the theoretical calculation in Eq. (12) of Supplemental Materials for different modes n. (C-E) Relaxation time of mode 2 under different parameters: (C) temperature, (D) model spring equilibrium length l_0, (E) persistence length l_p. Black lines are theoretical calculations from Eq. (12) of Supplemental Materials. (F) Test of equipartition of energy among modes for a filament of length 1 µm. Mean value of of coefficients $\langle \mathbf{q}_n{}^2 \rangle$ compared with the theoretical value in Eqs. (15) and (16) of Supplemental Materials.

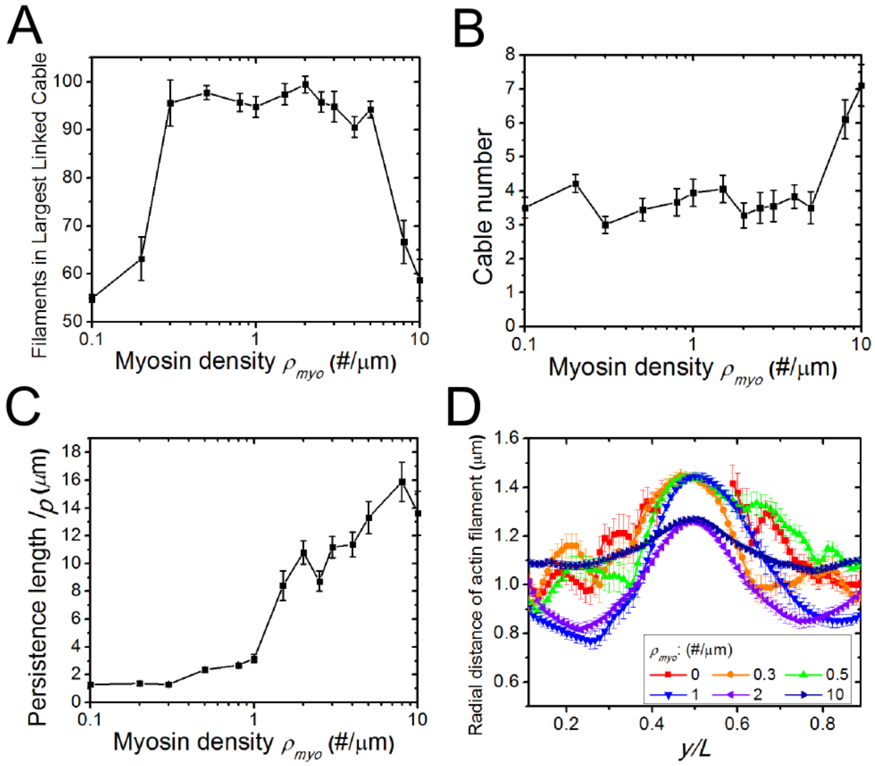

Figure S3. Myosin V walking along actin filaments influences cable thickness and stiffness. All parameters other than ρ_{myo} are given in Table S1. Error bars are SEM from 5 runs. (A) Thickest cable size as a function of ρ_{myo}. At low ρ_{myo}, actin filaments are not able to span the whole cell and form a connected structure near cell tips that contains ~55 filaments. At intermediate ρ_{myo} the filaments extend through the middle and can form a connected structure that contains ~ 95 filaments. At the highest ρ_{myo}, myosin pulling unbundles the filaments, resulting in smaller values for the thickest cable size. (B) Cable number as a function of ρ_{myo}. The total number of cables increases about 2-folds as ρ_{myo} increases. (C) Effective cable persistence length as a function of ρ_{myo}. The effective persistence length is the average persistence length of the filaments in the simulation, excluding filament segments within the semispherical cell tips. The persistence length grows from ~1.5 μm to more than 12 μm as myosin V density increases, suggesting a straightening effect due to pulling. (D) Graph of average radial distance of actin filaments along the long axis of the cell, *y/L*. At high ρ_{myo}, straightened actin cables are stretched closer to the nucleus.

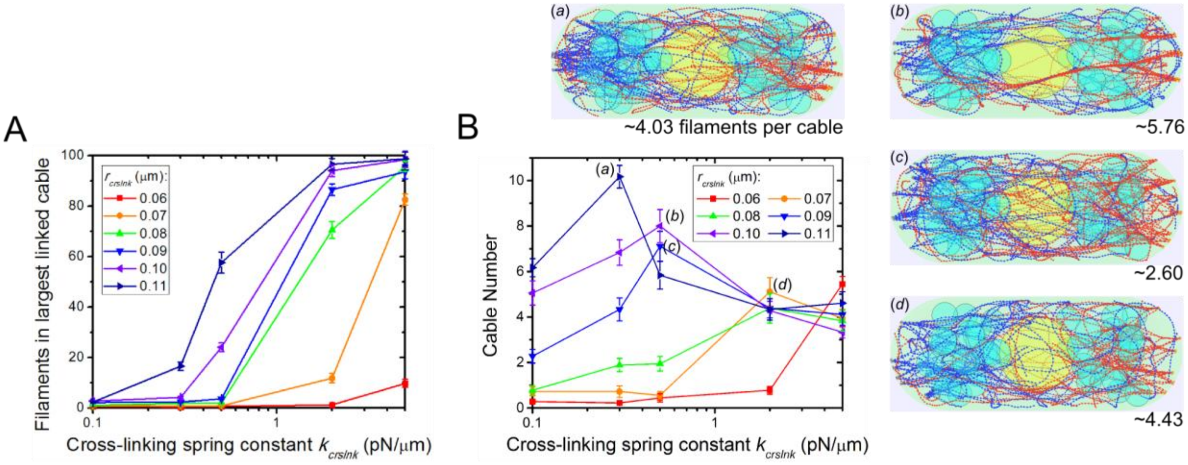

Figure S4. Modifying simulated cross-linking range r_{crslnk} and cross-linking spring constant k_{crslnk} affects actin cable thickness and number. All error bars are SEM from 5 runs. (A) Number of filaments in the thickest cable as a function of k_{crslnk} under different r_{crslnk}. Increasing r_{crslnk} and k_{crslnk} leads to thicker cables. (B) Cable number as a function of k_{crslnk} and r_{crslnk}. As k_{crslnk} increases from 0.1 pN/μm, it first causes unbundled filaments to come together in bundles. Further increase causes the bundles to merge into fewer but thicker cables. (a)-(d) Snapshots of simulations at peak positions in the graph.

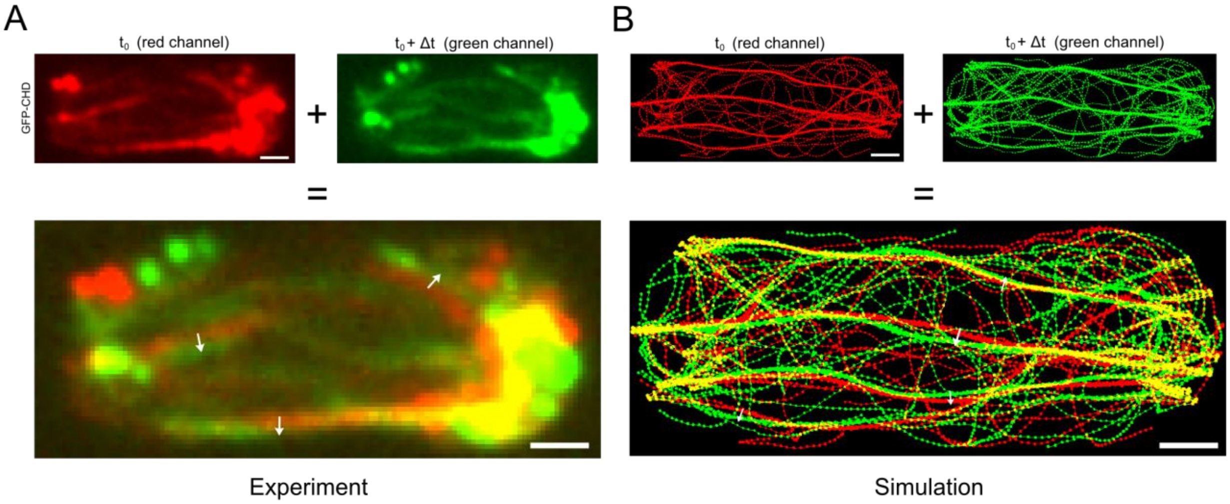

Figure S5. Measurement of lateral movement of actin cables in experiments and simulations. Red channel shows actin cables at time t_0 and green channel shows actin cables one frame later at $t_0+\Delta t$ of (A) GFP-CHD labeled actin filaments in experiments and (B) simulations. The two channels are merged to show the lateral movement per frame, which is calculated as the perpendicular displacement from the center of the red cable to the center of the green cable (arrows). If the cable remains stationary, the merged frame will show yellow, which is also counted. Scale bar: 1μm.

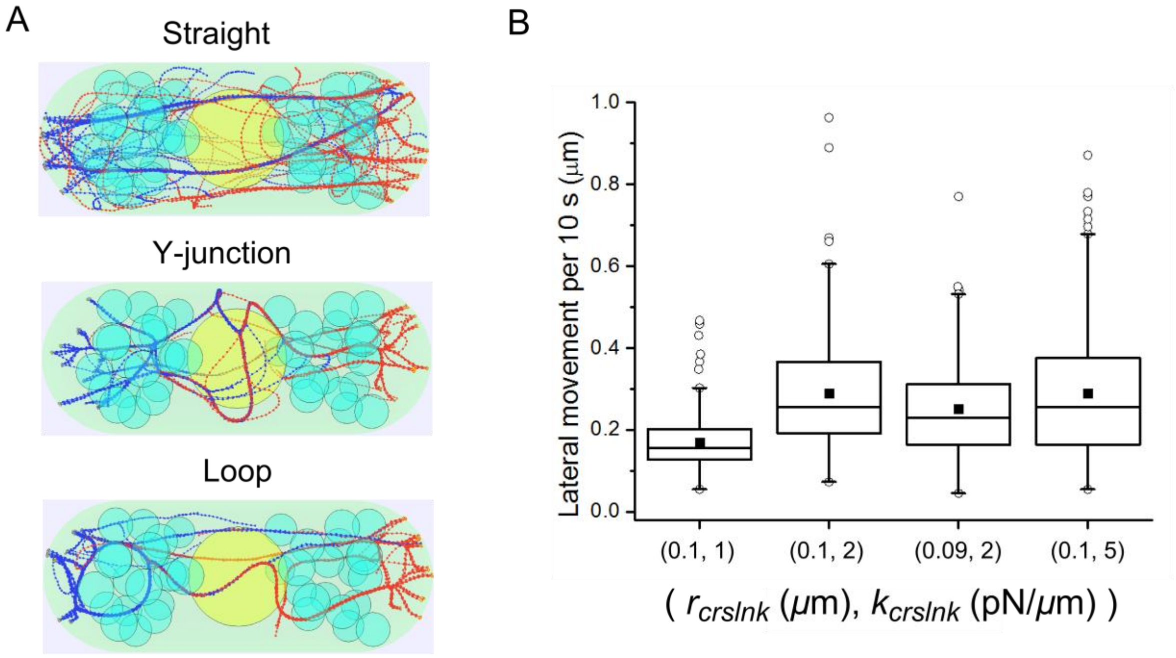

Figure S6. Examples of cable features and lateral movement in simulations. (A) Examples of simulated actin cables showing features: straight, Y-junctions and loops. (Top: r_{crslnk} = 0.1 µm, k_{crslnk} = 1.0 pN/µm; Middle and Bottom panel: r_{crslnk} = 0.1 µm, k_{crslnk} = 5.0 pN/µm). Y-junctions and loops are typical features of high k_{crslnk} cases where parallel cables are preferred and anti-parallel cables bulge and break. (B) Lateral movement of cables is measured upon varying (r_{crslnk}, k_{crslnk}), with values corresponding to the symbols shown in Figure 6F. Dots in graph indicate average values; boxes contain 50% of data; whiskers: 1.5 interquartile range.

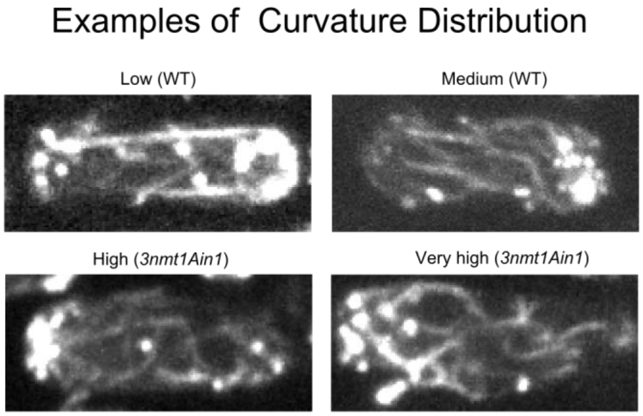

Figure S7. Evaluation of curvature distribution of actin cables. For every point along the contour of cables, we define the curvature κ to be: $\kappa = \left\| \frac{d\boldsymbol{t}}{ds} \right\| = \frac{1}{R}$, where $\boldsymbol{t}$ is the unit tangent vector, s is arc length and R is the radius of the circle of curvature. Low: cables are straight and have small curvature (0 → 1/5 μm^{-1}), example from WT. Medium: cables with higher average curvature (1/5 → 1/3 μm^{-1}), WT. High: cables are curved, curvature distribution has values (1/3 → 1/1.5 μm^{-1}), *3nmtAin1* cells. Very high: curvatures have values larger than 1/1.5 μm^{-1}. Most cables are highly curved in *3nmtAin1* mutants. In the simulations of Fig. 6F, curvature was calculated as in experimental images, using images of cells obtained after 140 s of simulation time.

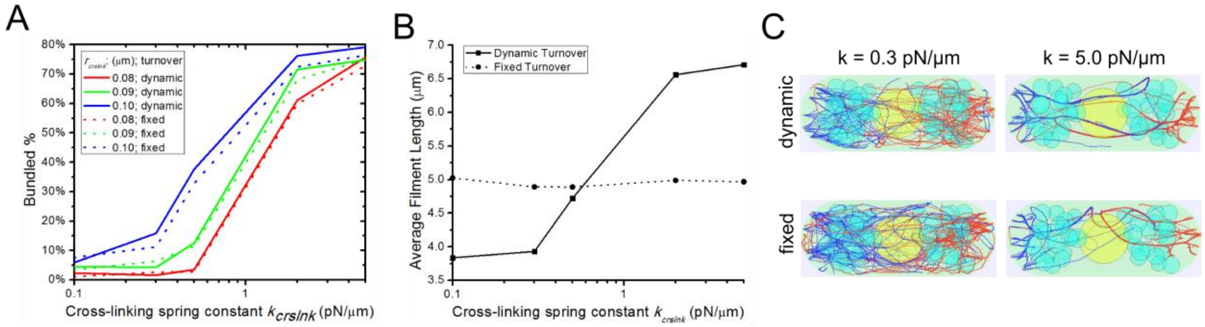

Figure S8. Comparison of simulations with cross-linker-dependent actin filament turnover rate to simulations with fixed turnover rate. In simulations with fixed turnover, the turnover rate was 1/15 s^{-1}. In the simulations with dynamic turnover this rate changed from 1/10 s^{-1} to 1/20 s^{-1} depending on the total bundled filament length, see section 4 of Supplemental Text. (A) Similar bundled percentage for fixed (dotted line) and dynamic (solid line) turnover rate as a function of cross-linking range r_{crslnk} and k_{crslnk}. (B) Average filament length remains constant for fixed turnover rate (dotted line). Compared to the fixed turnover case (dotted line), the average filament length is shorter at low k_{crslnk} and longer at high k_{crslnk} for dynamic turnover rate (solid line). (C) Images of simulations showing effects described in panel B.

SM Table

Table S1. Complete Table of Model Parameters.

Parameter	Description	Value	Unit
N	Number of the formins at one tip (total 2N)	72	
$N_{cluster}$	Number of clusters at one tip	12, 4→72	
$\rho_{cluster}$	Cluster density, $\rho_{cluster}= N/N_{cluster}$	6, 1→18	
D_{yeast}	Diameter of yeast cell	3.6	µm
L_{yeast}	Length of yeast cell	9	µm
N_{vac}	Number of vacuoles	40	
D_{vac}	Diameter of vacuole	0.8	µm
D_{nuc}	Diameter of nucleus	2.4	µm
v_{pol}	Polymerization rate (barbed end growth)	0.3	µm/s
$v_{pointed}$	Pointed end growth/shrinking rate	0	µm/s
τ_{sever}	Average turnover time	15	s
l_{sever}	Severing characteristic length, $l_{sever}= v_{pol}\ \tau_{sever}$	4.5	µm
T	Temperature	300	K
l_p	Persistence length of actin filaments	10	µm
κ	Flexural rigidity, $\kappa = k_B T\ l_p$	0.0414	pN·µm^2
l_0	Filament model segment length	0.1	µm
k	Spring constant	100	pN/µm
η	Cytoplasmic viscosity (350 times larger than water)	0.301	pN/µm^2·s
k_{crslnk}	Cross-linking spring constant	2, 0→15	pN/ µm
r_0	Cross-linking gap distance	0.03	µm
r_{crslnk}	Cross-linking interaction range	0.09, 0→0.16	µm
F_{myo}	Myosin walking force	0.5	pN
ρ_{myo}	Myosin linear density along filament	1, 0→10	#/µm
λ_{myo}	Myosin force density, $\lambda_{myo}= F_{myo}{*}\ \rho_{myo}$	0.5, 0.5→5	pN/µm
τ_{myo}	Myosin V lifetime on actin filament	5	s

SM Videos

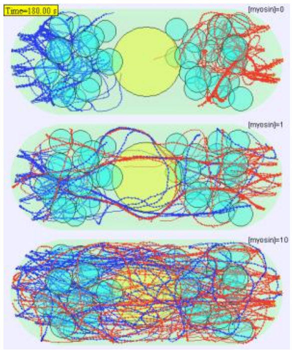

Video 1. Myosin V density ρ_{myo} (#/µm) affects actin cable structure (see Figure 3 and Figure S3). In simulations that lack of myosin pulling force, the cables are not able to span the entire cell, creating thick and curved cables. Increasing ρ_{myo} stretches the cables, enabling them to connect with cables from the opposite end. At ρ_{myo} = 10/µm, the pulling is strong and cables become straight and less bundled.

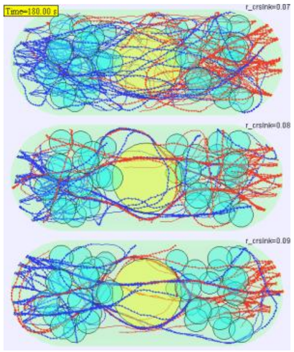

Video 2. Increasing r_{crslnk} bundles actin filaments (see Figure 4 and Figure S4). At r_{crslnk} = 0.07 µm, 15% of the total actin filaments are bundled, compared to 59% and 68% at r_{crslnk} = 0.08 µm and r_{crslnk} = 0.09 µm.

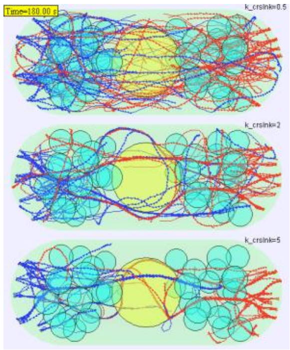

Video3. Increasing k_{crslnk} bundles actin filaments in a parallel fashion (see Figure 4 and Figure S4). At k_{crslnk} = 0.5 pN/µm, 9% of the total actin filaments are bundled, compared to 69% and 74% at k_{crslnk} = 2 pN/µm and k_{crslnk} = 5 pN/µm. Anti-parallel cables at k_{crslnk} = 5 pN/µm undergo buckling, bulging and breaking.

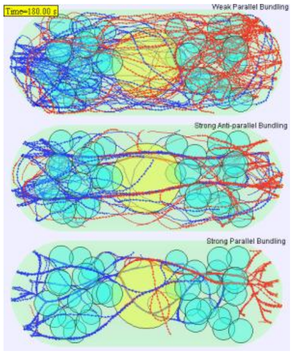

Video 4. Bundling mechanisms under different (r_{crslnk}, k_{crslnk}) parameter sets (corresponds to Figure 4*D*, Figure 5 and Figure S5). Simulation (r_{crslnk}, k_{crslnk}) at (0.07, 5), (0.1, 1), (0.1, 5) show features discussed as weak parallel bundling, strong anti-parallel bundling and strong parallel bundling. Units of (r_{crslnk}, k_{crslnk}): (µm, pN/µm).